Chain Architecture Effects on the Diffusion of Cylinder-Forming Block Copolymers

V. Khanna,[†] B. J. Kim,[‡] A. Hexemer,[†] T. E. Mates,[†] E. J. Kramer,*[,†,‡] X. Li,[§] J. Wang,[§] and S. F. Hahn[⊥]

Department of Materials, University of California, Santa Barbara, California 93106; Department of Chemical Engineering, University of California, Santa Barbara, California 93106; Advanced Photon Source, Argonne National Laboratory, Illinois 60439; and Performance Plastics and Chemicals, The Dow Chemical Company, Freeport, Texas 77541

Received July 26, 2006; Revised Manuscript Received November 27, 2006

ABSTRACT: We investigate the effect of chain architecture on the self-diffusion of poly(styrene)−poly(ethylene) triblock (PS−PE−PS or SES) and pentablock (PS−PE−PS−PE−PS or SESES) copolymers with a cylindrical domain structure (E cylinders). Transmission electron microscopy (TEM) and grazing-incidence small-angle X-ray scattering (GISAXS) are employed to reveal the microstructure of the block copolymer films, and dynamic secondary ion mass spectroscopy (DSIMS) is used to obtain diffusion coefficients. The triblock copolymer (SES) chains diffuse through a randomly oriented cylindrical structure via a "hopping" mechanism where the normalized diffusion coefficient D/D_0 (D is the diffusion coefficient of the block copolymer and D_0 is the diffusion coefficient of a disordered (hypothetical) block copolymer of similar M_w) decreases exponentially with the thermodynamic barrier χN_{PE}, where χ is the Flory interaction parameter between styrene and ethylene and N_{PE} is the degree of polymerization of the poly(ethylene) block. However, the pentablock copolymer (SESES) diffuses via a "walking" mechanism through an ordered cylindrical structure which involves the activation of a single E block at a time to overcome the thermodynamic barrier. Both mechanisms have been reported previously for diblock and triblock copolymers, respectively. Hence, for a similar overall M_w the pentablock copolymer diffuses faster than the corresponding triblock copolymer. Moreover, a comparison is made between perpendicular and parallel diffusion in the pentablock copolymer as both mechanisms are observed due to a change in the cylinder orientation (from parallel to perpendicular cylinders) as a function of depth. The relative independence of the parallel diffusion on χN_{PE} suggests that the thermodynamic barrier for perpendicular diffusion does not affect parallel diffusion coefficients. However, the normalized parallel and perpendicular diffusion coefficients of the SESES pentablock copolymer as well as the normalized perpendicular diffusion coefficient of the SES triblock copolymer are substantially less than the corresponding diffusion coefficients of a cylinder-forming diblock copolymer investigated by Cavicchi and Lodge at the same values of χN_{cyl}, where N_{cyl} is the degree of polymerization of the cylinder block. This comparison suggests that entangled loops in the PE midblock cylinders impose additional entropic barriers to diffusion that are absent for diblock copolymers.

Introduction

The ability of block copolymers to segregate into nanoscale morphologies makes them an extremely versatile class of materials for a number of engineering and technological applications.[1−3] However, the usefulness of these materials in any practical application depends on the structure (morphology and chain architecture) as well as their rheological properties which, in turn, are closely related to their diffusion kinetics. The segregated nanoscale structure of a block copolymer, due to its composition, block length, and the Flory parameter χ, is analogous to a periodic potential field that a diffusing block copolymer chain will encounter. The orientation of the microdomains as well as the extent of order in the structure determines the nature of this potential field.

The diffusion of block copolymers with a symmetric composition producing, in turn, a lamellar morphology has been extensively investigated previously. In an ordered structure with a lamellar morphology, a diffusing block copolymer chain sees a uniform potential when diffusing parallel to the lamellae but a periodic potential when diffusing perpendicular to the lamellae. Mean field theory calculations by Fredrickson and Milner showed that the diffusion of a tracer block copolymer or homopolymer into a weakly ordered lamellar phase is considerably impeded due to the spatially periodic chemical potential exerted by the matrix.[4] Barrat and Fredrickson also reported numerical simulations which showed that the tracer diffusion in a symmetric diblock copolymer was slowed down in both strongly and weakly segregated structures.[5] However, they reported that the suppression of self-diffusion near the order−disorder transition temperature is modest relative to that observed in a strongly segregated lamellar structure. Moreover, they also reported that self-diffusion (i.e., tracer is identical to the matrix) is also suppressed by the chemical potential of the matrix. For sufficiently entangled block copolymers, the effect of entanglements on parallel diffusion must be considered. Shull et al. observed that self-diffusion into symmetric poly(ethylenepropylene)-*block*-poly(ethylethylene) copolymer (PEP−PEE) diblock copolymer films depends on the thermal history of the film. Diffusion in as-cast films was characteristic of diffusion in a uniform medium whereas that in preannealed films was reduced considerably.[6] They suggested that the latter was observed due to the parallel orientation of the lamellar sheets in the films which forces the chains to diffuse perpendicular to the sheets. Dalvi and Lodge measured the diffusion anisotropy

* Corresponding author: e-mail edkramer@mrl.ucsb.edu; Tel (805) 893-4999.
[†] Department of Materials, University of California.
[‡] Department of Chemical Engineering, University of California.
[§] Argonne National Laboratory.
[⊥] The Dow Chemical Company.

10.1021/ma061703p CCC: $37.00
Published on Web 03/03/2007

in lamellar block copolymers for the same system as a function of the diffusion direction (parallel to the lamellae and perpendicular to the lamellae).[7] Lodge and Dalvi proposed a block retraction mechanism for diffusion parallel to the interface.[8] This mechanism involves the retraction of one block through the entanglements into the interface between lamellae and then reextending out into a new configuration. Irrespective of the entanglement structure, diffusion perpendicular to the lamellar interfaces is always affected by the thermodynamic barrier χN, where N is the total degree of polymerization of the symmetric AB diblock copolymer since each block has to overcome the barrier due to $N/2$ contacts with the other block to diffuse in the perpendicular direction. The idea that one block will try to minimize the number of contacts it makes with distinct chemical units while diffusing perpendicularly through the other block was suggested by Helfand.[9] Using molecular dynamics simulations, Murat et al. confirmed that the diffusion perpendicular to the lamellar interfaces is strongly dependent on the Flory parameter χ, whereas the diffusion parallel to the interfaces does not show any significant dependence on χ.[10]

For cylindrical block copolymers in the hexagonal packing, trends similar to those found for lamellar block copolymers have been observed. No anisotropy of diffusion was observed parallel to vs perpendicular to the cylinders for entangled PEP−PEE samples[11] whereas for a PEO−PEE samples diffusion anisotropy has been reported along and across the cylinder interfaces.[12] However, using photon correlation spectroscopy, Vogt et al. also observed that about 50 K below the order−disorder transition the dynamics of a poly(styrene)-*block*-poly(methylphenylsiloxane) diblock copolymer were controlled by the translational motion of the PS cylinders in the mobile poly(methylphenylsiloxane) matrix.[13] Finally, Cavicchi and Lodge have recently shown that the defect structure in a cylindrical block copolymer strongly affects the diffusion perpendicular to the cylinder interfaces.[14] They reported that, for a well-aligned sample, the parallel diffusion follows a block retraction mechanism, mentioned earlier for the lamellar block copolymers. For misaligned samples, they observed that the perpendicular diffusion coefficient increased with increases in the amount of misaligned cylinders and dislocations. However, the parallel diffusion coefficient did not show a strong dependence on the defect structure.

In a series of papers Yokoyama et al. have investigated the melt diffusion kinetics of asymmetric PS−PVP block copolymers with a spherical morphology using forward recoil spectrometry (FRES) and dynamic secondary ion mass spectroscopy (DSIMS). They observed that for dPS−PVP diblock copolymers the diffusion kinetics were reduced considerably with respect to the diffusion of PS homopolymer with the same degree of polymerization.[15] They attributed this reduction to the free energy barrier that exists due to the ordered structure of the diblock copolymer and suggested a hopping diffusion mechanism where the kinetics are controlled by the barrier to the movement of individual PVP blocks (PVP is the minority block) from one spherical domain to the other. By investigating diffusion kinetics in thin films of the same block copolymers, they extracted a hopping frequency or a characteristic hopping time which compared well with the time scales obtained from much longer range diffusion in the previous work.[16] Furthermore, by investigating the diffusion of thin diblock copolymer films into mixtures of diblock copolymers and homopolymers (PS), they studied the effect of the structure (ordered or disordered) on the diffusion of the block copolymer.[17] They observed that the diffusion mechanism undergoes a transition from the activated hopping mechanism to the Stokes−Einstein diffusion as the structure undergoes a change from an ordered spherical structure to a dilute disordered arrangement of spherical micelles. They compared the self-diffusion and tracer diffusion of triblock copolymers and diblock copolymers.[18] For similar block lengths, the diffusion kinetics were similar for the two architectures. However, for similar total molecular weights, the triblock copolymer diffused much faster. Simulations on diblock and triblock copolymer melts (using both Rouse and reptation dynamics) corroborated these experimental results.[19] Last, they also studied the mutual diffusion of diblock and triblock copolymers in homopolymers.[20] They attributed the differences in the diffusion coefficients of the diblock/homopolymer combination and the triblock/homopolymer combination to the presence of bridging chains in triblock copolymers which limited the mutual diffusion.

In a previous paper on the mechanical properties of thin films of poly(cyclohexylethylene)−poly(ethylene) (PCHE−PE) block copolymers, it was reported that the ordering kinetics of a pentablock copolymer were considerably slower than that of a triblock copolymer with larger block lengths.[21] It could not be stated with conviction whether slower diffusion kinetics of the pentablock architecture (as compared to the triblock architecture) was responsible for this behavior or whether the difference in kinetics reflects a different thermodynamic driving force for the orientation. The aim of this work is to study the effect of triblock vs pentablock chain architecture on the diffusion of block copolymers albeit in a different system. Two asymmetric poly(styrene)-*block*-poly(ethylene) copolymers with a cylindrical morphology and different architectures, triblock (SES) and pentablock (SESES), are used for the studies. Dynamic secondary ion mass spectroscopy has been used to depth profile isotopically labeled block copolymers after allowing them to diffuse into their unlabeled preannealed ordered counterparts. The microstructure of the preannealed films is characterized by transmission electron microscopy (TEM) and grazing-incidence small-angle X-ray scattering (GISAXS). The self-diffusion coefficients at different temperatures are measured and compared for the two architectures in order to understand how the structure of the block copolymer affects the diffusion. Moreover, in the pentablock copolymer SESES, a change in diffusion mechanism is observed as a function of depth due to a change in cylinder orientation (from parallel to perpendicular) in the preannealed films. This allows for a comparison of perpendicular and parallel diffusion in the pentablock copolymer.

Experimental Section

Materials. The diffusion couples are made of poly(styrene)−poly(ethylene)−poly(styrene) (SES) and poly(styrene)−poly(deuterated ethylene)−poly(styrene) (SdES) and their pentablock counterparts, i.e., SESES and SdESdES. The block copolymers have an overall poly(ethylene) (E) weight fraction f_E (or f_{dE}) of 0.25 and thus form a cylindrical domain structure where the PE cylinders are embedded in a PS matrix. The block copolymers were synthesized by sequential anionic polymerization to yield poly(styrene)−poly(butadiene)−poly(styrene) (SBS) and poly(styrene)−poly(butadiene)−poly(styrene)−poly(butadiene)−poly(styrene) (SBSBS) block copolymers followed by hydrogenation (or deuteration) to convert the PB block to PE (or PdE). The PE blocks contained an average of 26 ethyl branches per 1000 backbone carbons. This was due to the 10% 1,2 monomer addition in the PB block. The deuterated and protonated counterparts for the triblock and the pentablock copolymer were matched in degree of polymerization and composition. The molecular weights and compositions of the block copolymers used are listed in Table 1.

Sample Preparation for Diffusion Measurements. Diffusion couples consisting of 35 nm thick top layers of the deuterated block

Table 1. Molecular Weight, Composition, and Block Lengths of the Block Copolymers Used in the Study

polymer	chain architecture	M_w (g/mol)	f_{PE} (wt %)	PS block (g/mol)	PE block (g/mol)
SES	triblock	50 000	25	18 750	12 500
SESES	pentablock	70 000	25	17 500	8 750

copolymers on thick (~800 nm) bottom layers of the protonated counterparts were prepared by spin-casting films from hot decahydronapthalene solutions. For the thick bottom layers an 8 wt % concentrated solution was used. The films were spin-cast onto hot Si substrates at 2500 rpm for 40 s. The films were then preannealed under high vacuum ($<10^{-7}$ Torr) at 230 °C for 24 h to obtain a completely segregated cylindrical microstructure. For the thin deuterated top layers, spin-casting was done from 0.7 wt % concentrated solutions onto NaCl substrates. The films were dried in low vacuum ($\sim 10^{-2}$ Torr) and subsequently floated off the substrates onto the surface of a deionized water bath. The floating films were picked up on top of the thick preannealed protonated block copolymer films.

The diffusion couples were then annealed at different temperatures and times. The diffusion times for any temperature were chosen to ensure sufficient diffusion of the top thin layer into the bottom thick layer and, at the same time, ensure that the diffusing species are still far away from the Si to minimize any effect that the substrate would have on the experiment. For dynamics SIMS analysis the samples were covered by a sacrificial layer of PS (M_n = 207K g/mol, 150 nm thick) by floating it onto the diffusion couple after the diffusion anneal from the surface of a water bath.

Transmission Electron Microscopy (TEM) Sample Preparation and Imaging. Cross-sectional TEM of the thin films was done in order to characterize the orientation of the microdomains. The films were floated off the NaCl substrates onto epoxy substrates. The films were then stained in RuO_4 vapor for 12−24 h. A 0.5% RuO_4-stabilized solution, obtained from Electron Microscopy Sciences, was used for the purpose. The ruthenium tetroxide selectively stains the PS matrix and the PE cylinders appear white in the TEM images. The staining was followed by capping of the films with another layer of epoxy. 100 nm thick cross sections of the films were microtomed at room temperature using a Leica Ultracut UCT ultramicrotome and a diamond knife. The cross sections were imaged using an FEI-T20 TEM operated at 200 keV.

GISAXS Measurements. The GISAXS measurements were performed at XOR-Sector 8 at the Advanced Photon Source (APS) at Argonne National Laboratory (ANL). A monochromatic X-ray beam of 7.4 keV energy (wavelength (λ) = 0.1675 nm) was used. The beam size was 160 μm × 55 μm. The sample-to-detector distance was 1915 mm. It was calibrated with silver behenate, which has a periodicity of 58.376 Å. A piece of lead was used as a beam stop. The incident angle α_i relative to the film sample surface was varied from 0.04° to 0.19° (the polymer critical angle α_c = 0.16°). The data were typically collected for 10−30 s exposure, depending on the beam intensity and a sum of 5−10 exposure images was taken for analysis. The images obtained were 2048 × 2048 pixels in 16 bit TIFF format. Each pixel was 79 μm × 79 μm.

Dynamic Secondary Ion Mass Spectroscopy. The DSIMS experiments were performed using a Physical Electronics 6650 instrument. Negative ions are detected as polymer is sputtered by an incident beam of 3 keV O_2^+ ions. The beam is rastered over a 250 μm region and negative ions of C, H, D (= ^{2}H), Cl, and Si from the center 15% of the crater area were monitored as a function of time. Under the conditions mentioned above, a depth resolution of about 9 nm is obtained. The sputtering time is converted to depth using the known thickness of the top PS sacrificial layer and the time taken to sputter through this layer.

Results

SES Triblock Copolymer. Block Copolymer Morphology and Microdomain Orientation. Cross-sectional TEM and GISAXS was used to reveal the morphology and microdomain orientation of the block copolymer in the thick film substrates. Figure 1a shows a cross-sectional TEM image of a triblock copolymer film preannealed at 230 °C for 1 day. The morphology of the block copolymer is cylindrical with PE cylinders embedded in a PS matrix. The cylinders are in a random arrangement with little lateral and depth order. Figure 1b shows a GISAXS diffraction pattern that corroborates this observation for the block copolymer film. The GISAXS diffraction pattern is for an incident angle α_i (= 0.21°) above the critical angle α_c ~ 0.167° for the polymer. A diffuse first-order ring is observed for the annealed film, suggesting the random orientation of the cylinders. The peak occurs at q^* = 0.24 nm^{-1}, which corresponds to a d_{10} spacing of 26.2 nm. The film does not show any improvement in order even after annealing for 6 days. The large M_w of the block copolymer results in extremely slow ordering kinetics, and hence the random orientation persists for times greatly in excess of the diffusion annealing times even though it is not the equilibrium morphology.

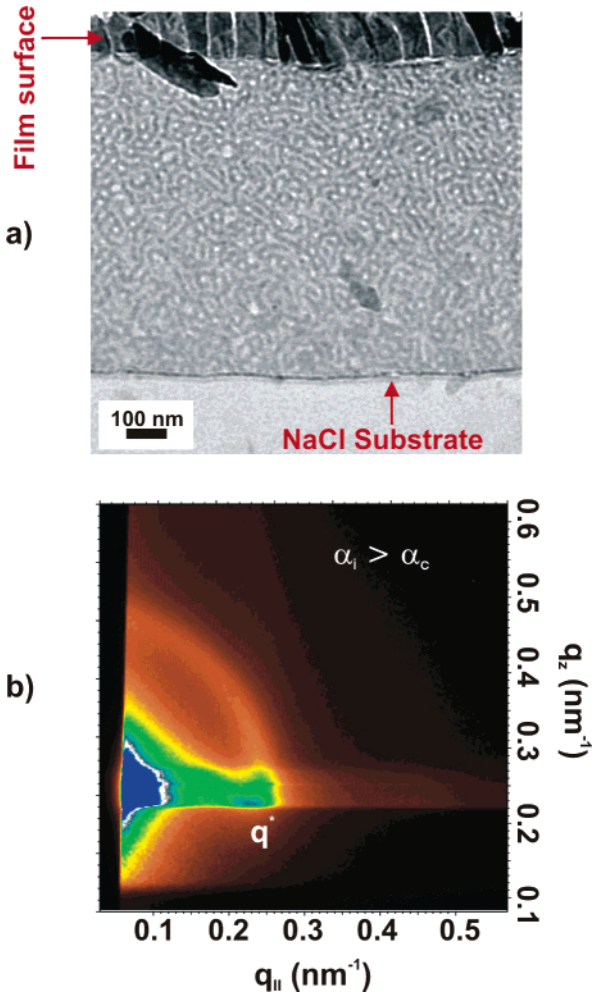

Figure 1. (a) Cross-sectional TEM micrograph and (b) GISAXS pattern at an incident angle of 0.21°, λ = 0.1675 nm, of $SES_{70.25}$ annealed at 230 °C for 1 day.

Diffusion Measurements of SES Triblock Copolymer. Figure 2a shows a typical normalized deuterium intensity vs depth plot of the deuterium signal from the PE block of SdES after annealing at 210 °C for 7 h. The diffusion profiles were fitted to a function consisting of a four error functions, corresponding to the solution for the diffusion of two species, volume fractions f and $(1 - f)$ and diffusion coefficients D_1 and D_2, respectively, from a film of thickness h

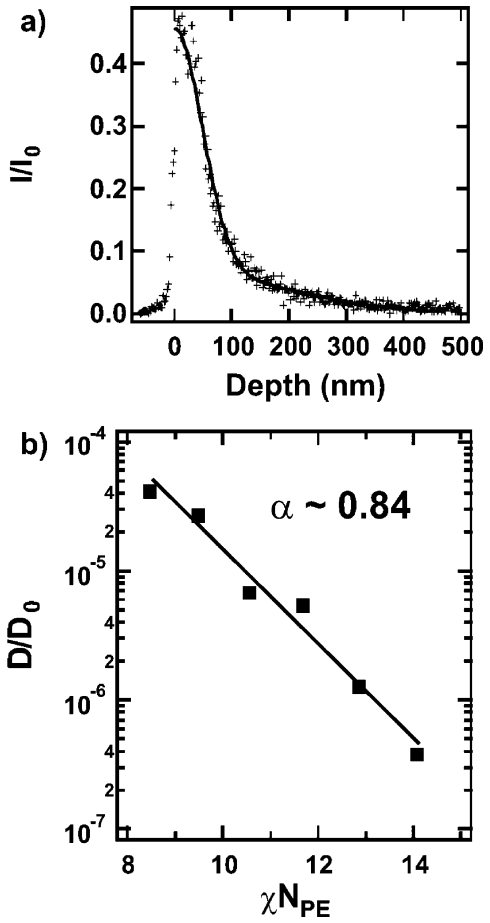

Figure 2. (a) SIMS depth profile of SdES triblock copolymer diffusing into a randomly oriented cylindrical domain structure of SES at 210 °C. The block copolymer was allowed to diffuse for 7 h. The solid line is the best fit using eq 1. (b) χN_{PE} dependence of the normalized self-diffusion coefficients D/D_0 for SES. D_0 is the diffusion coefficient of polystyrene with a similar M_w at the temperature. The solid line is the fit using eq 3.

$$I = I_0\left[f\left(\mathrm{erf}\frac{h-x}{2\sqrt{D_1 t}} + \mathrm{erf}\frac{h+x}{2\sqrt{D_1 t}}\right) + (1-f)\left(\mathrm{erf}\frac{h-x}{2\sqrt{D_2 t}} + \mathrm{erf}\frac{h+x}{2\sqrt{D_2 t}}\right)\right] \quad (1)$$

where t is the annealing time and I_0 is a scaling factor. A weighted average diffusion coefficient is reported

$$D = fD_1 + (1-f)D_2 \quad (2)$$

The two diffusion coefficients are needed to achieve a good fit because of the residual polydispersity of the block copolymers as demonstrated previously for spherical block copolymers.[15] From the TEM images, the structure of the triblock copolymer in the thick film consists of short, disordered cylinders of PE embedded in a matrix of PS. The diffusion mechanism would be the hopping motion of individual chains from one cylinder to another; i.e., the diffusion coefficient would be the same as that for diffusion perpendicular to a well-oriented array of cylinders (D_{per}). The free energy barrier for this mechanism χN_{PE} (N_{PE} is the number of segments of the shorter PE block), and the diffusion coefficients are scaled by

$$D \sim D_0 \exp(-\alpha\chi N_{PE}) \quad (3)$$

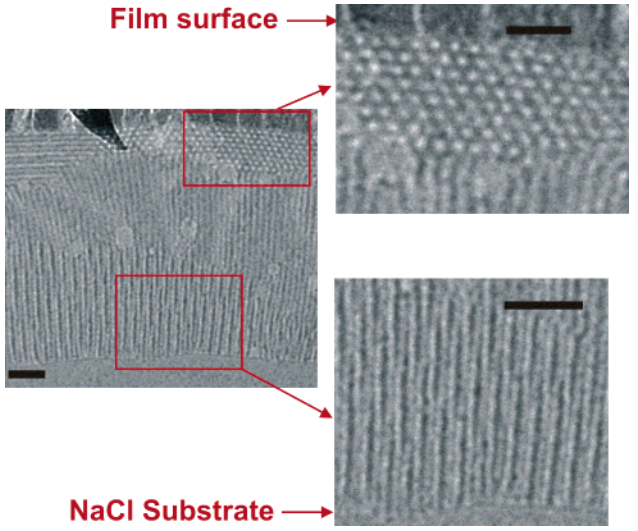

Figure 3. Cross-sectional TEM micrograph of SESES annealed at 230 °C for 1 day. The scale bars on the TEM images are 100 nm. The top and bottom portions of the film are shown to highlight the difference in cylinder orientation through the film thickness.

where D_0 is the hypothetical diffusion coefficient in the disordered phase and the constant α is determined by the complete free energy barrier for the diffusion mechanism. The temperature-dependent Flory parameter $\chi(T)$ for poly(styrene)−poly(ethylene) was obtained from ref 22 and is given by

$$\chi(T) = \frac{114.3}{T} - 0.1893 \quad (4)$$

To obtain the fits, D_0 was set as the diffusion coefficient of polystyrene homopolymer of total M_w similar to the block copolymer at the required temperature. It should be noted here that D_0 has a WLF temperature dependence.[24] This choice of D_{PS} for D_0 is based on the consideration that poly(styrene) with a T_g of 100 °C is the slower diffusing species of the two blocks. Support for this assumption also comes from a comparison of the diffusion coefficients of linear poly(ethylene) and poly(styrene). At 175 °C, linear PE (M_w = 32K g/mol) has a diffusion coefficient of about 2×10^{-9} cm^2/s,[23] whereas for comparable PS (M_w = 55K g/mol) at the same temperature, the reported value is about 5×10^{-14} cm^2/s.[24] This assumed value of D_0 thus produces a D/D_0 that is an upper limit but one that seems reasonable on the basis of the fact that the elementary hopping step involves motion of isolated short midblock PE chains through the higher-T_g PS end block matrix. For triblock copolymers with the PE midblock forming the core of the cylinders, diffusion would involve the pullout of the PE block from the core of one cylinder into the PS matrix and entry into the next. The thermodynamic penalty would simply be χN_{PE} due to the unfavorable contacts between the PE block and the PS matrix. To obtain the value of α, the log of the normalized diffusion coefficients (D/D_0) are plotted as a function of χN_{PE}, as shown in Figure 2b, and the best fit is obtained for α ~ 0.84. This value is reasonably close to unity, the expected value for activated hopping through an ordered hexagonal array of cylinders with their axis aligned parallel to the film plane (which would be equivalent to a close packed bcc arrangement of spheres). The slightly reduced value of α may be due to the diffuse nature of the PS−PE interface.

SESES Pentablock Copolymer. Block Copolymer Morphology and Microdomain Orientation. Contrary to what is observed for the triblock copolymer, the pentablock copolymer

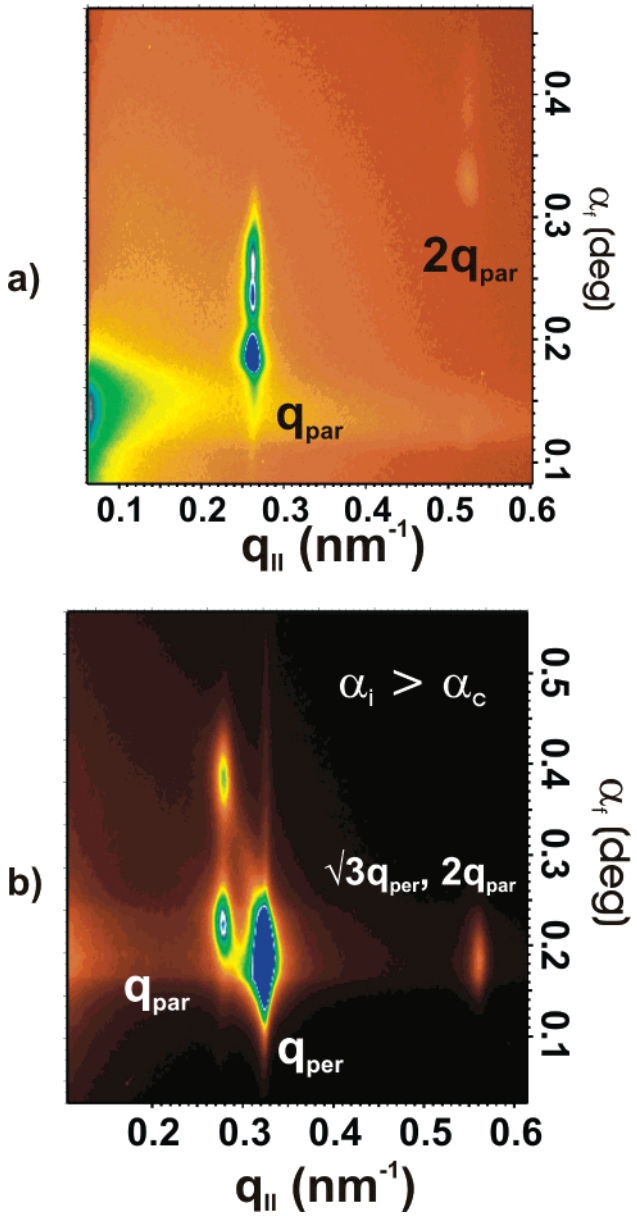

Figure 4. GISAXS pattern ($\lambda = 0.1675$ nm) at an incident angle of (a) 0.04° and (b) 0.19° of SESES annealed at 230 °C for 1 day.

SESES, shows an ordered orientation of the cylindrical microdomains when annealed at 230 °C for 1 day. However, the orientation undergoes a change with depth (Figure 3). The top 140 nm of the film shows a preferred orientation of the cylinders with their axes parallel to the film plane. This corresponds to about eight layers of cylinders. Inside the film, however, the cylinders prefer to align with their axes perpendicular to the film plane. Figure 4a show the GISAXS diffraction pattern for an incident angle α_i (= 0.04°) below the critical angle $\alpha_c \sim 0.167°$ for the polymer. Under these conditions two sets of peaks are observed with $q_{||}$ coordinates $q_{par} = 0.277$ nm^{-1} and $2q_{par}$. Since at this angle the X-rays are only scattered significantly from the top 2 or 3 layers of cylinders with close packed (10) planes parallel to surface, the q_{par} peaks arise from (10) planes tilted at 60° to the surface. The magnitude of the q_{par} component (= 0.277 nm^{-1}) of the reciprocal lattice vector corresponds to a (10) plane spacing of 19.6 nm. In the GISAXS diffraction patterns above the critical angle ($\alpha_i = 0.19°$, Figure 4b) in addition to the q_{par} set of peaks a much more intense peak (q_{per}) is observed along the $q_{||}$ direction. This peak, whose $q_{per} = 0.32$ nm^{-1} corresponds directly to the (10) plane spacing of 19.6 nm inferred from the diffraction from surface layers of parallel cylinders, comes from scattering from cylinders aligned perpendicular to the surface but lying well below the set of parallel layers of cylinders at the surface. These GISAXS results corroborate the TEM results which show that the parallel orientation persists in the top layers of the block copolymer film and that below these layers the perpendicularly oriented cylinders exist. Annealing the film for 10 days at the same temperature does not result in a change in orientation of the cylinders. The number of layers of lying down cylinders is about the same, and below them the perpendicular orientation is observed throughout the film. This unusual orientation may result due to the neutrality of the substrate for the PS and PE blocks and the preference of the surface for the PE block ($\gamma_{PE,220°C}$ (68K g/mol) = 20.9 mJ/m^2,[25] $\gamma_{PS,220°C}$ (21K g/mol) $\sim$ 27 mJ/m^2 [26]).

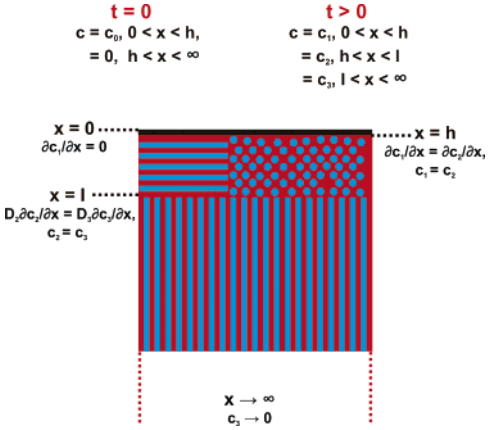

Figure 5. Film schematic showing the boundary conditions for the solution to eq 5. The black layer on the surface is the thin film diffusing into the thick film with a mixed orientation of cylinders.

Diffusion Measurements of SESES. The unusual orientation of the cylindrical microdomains in the SESES block copolymer films (as described in the previous section) makes it possible to study the diffusion of SdESdES chains in both directions parallel and perpendicular to the cylindrical axis. The resolution of D-SIMS allows us to extract a diffusion coefficient from the top 120−140 nm of the film (cylindrical axes aligned parallel to the film plane, perpendicular diffusion, D_{per}), whereas the rest of the film, which has a preferred perpendicular orientation of the cylinders, makes it possible to extract a diffusion coefficient parallel to the cylindrical axes (D_{par}). In order to obtain D_{per} and D_{par} for the block copolymer, the equation for Fick's second law of diffusion, i.e.

$$\frac{\partial C}{\partial t} = D\frac{\partial^2 C}{\partial x^2} \tag{5}$$

was solved for the three different regions, $0 \le x \le h$ (initial SdESdES layer), $h \le x \le l$ (parallel cylinder layers), and $l \le x < \infty$ (perpendicular cylinder layers). The continuity of flux at $x = h$ and $x = l$ along with the constraint that there is no flow of diffusing substance through the top surface were the five boundary conditions used to solve eq 5. Last, it was assumed that the concentration goes to zero as $x \rightarrow \infty$. The method of Laplace transformation was employed to solve the equations. A schematic of the system along with the boundary conditions is shown in Figure 5.

The solutions are of the following form (see Appendix for detailed solution):

$$c_2(x,t) = -\frac{c_0}{2}\left[\mathrm{erf}\left(\frac{h+x}{2\sqrt{D_{\mathrm{per}}t}}\right) + \mathrm{erf}\left(\frac{h-x}{2\sqrt{D_{\mathrm{per}}t}}\right) - \sum_{n=0}^{\infty}(-\alpha_{an})^n\left\{\mathrm{erf}\left(\frac{2nl+h+x}{2\sqrt{D_{\mathrm{per}}t}}\right) + \mathrm{erf}\left(\frac{2nl+h-x}{2\sqrt{D_{\mathrm{per}}t}}\right) - \mathrm{erf}\left(\frac{2nl-h+x}{2\sqrt{D_{\mathrm{per}}t}}\right) - \mathrm{erf}\left(\frac{2nl-h-x}{2\sqrt{D_{\mathrm{per}}t}}\right)\right\}\right] \quad (6)$$

$$c_3(x,t) = \frac{c_0 k}{1+k}\sum_{n=0}^{\infty}(-\alpha_{an})^n\left\{\mathrm{erf}\left(\frac{(2n+1)l+h}{2\sqrt{D_{\mathrm{per}}t}} + \frac{x-l}{2\sqrt{D_{\mathrm{par}}t}}\right) - \mathrm{erf}\left(\frac{(2n+1)l-h}{2\sqrt{D_{\mathrm{per}}t}} + \frac{x-l}{2\sqrt{D_{\mathrm{par}}t}}\right)\right\} \quad (7)$$

Here, c_0 is the initial concentration confined in the thin film of thickness h, $c_2(x,t)$ is the concentration in the region in the thick film where the cylinders are oriented parallel to the film plane, i.e., where perpendicular diffusion occurs with a diffusion coefficient D_{par} and $c_3(x,t)$ is the concentration in the region $x > l$ where the cylinders are perpendicular to the surface with a diffusion coefficient D_{per}. Note that the quantity α_{an} is completely different from α in eq 3 and depends on the anisotropy of diffusion. It is defined by

$$\alpha_{\mathrm{an}} = \frac{1-k}{1+k} \quad (8)$$

$$k = \sqrt{\frac{D_{\mathrm{per}}}{D_{\mathrm{par}}}} \quad (9)$$

For the purpose of fitting c_0 was taken as 1, and the solution was multiplied by a scaling factor to scale the theoretical solution to the experimental data. The factor was not a separate fitting parameter but depended on the intensity of the peak in the experimental data. In the fitting procedure, h, l, and t were taken as constants ($h = 30$ nm, $l = 130$ nm, and t is the annealing time). The nonuniformity in thickness of the region with parallel cylinders (120−140 nm) makes the choice of $l = 130$ nm a reasonable one. For the perpendicular cylinder region, where the diffusion occurs parallel to the cylinders, the fit was obtained from 150 nm to the substrate to ensure that the region of fit is the region where the cylinders are only aligned perpendicular to the film. For all temperatures, the fits were independent of n for $n \geq 300$; hence, a sum of 300 terms was taken for the infinite series. In order to obtain a better fit for perpendicular diffusion, c_2 was taken as a sum of two solutions due to the residual polydispersity of the SdESdES block copolymer, as was done for the case of the triblock copolymer, i.e.

$$c_2 = f\,c_{21} + (1-f)c_{22} \quad (10)$$

where c_{21} and c_{22} are eq 6 with two different values of D_{per} and f was taken as a separate fitting parameter. Hence, the coefficient for perpendicular diffusion was calculated using

$$D_{\mathrm{per}} = f\,D_{\mathrm{per},c_{21}} + (1-f)D_{\mathrm{per},c_{22}} \quad (11)$$

For fitting the data for the region of parallel diffusion ($x > l$), only a single value of D_{par} was used. However, because of the finite thickness of the preannealed thick film, the deuterium signal does not decay completely to zero before the Si substrate is reached. In order to obtain a better fit eq 7 was modified, and $c_{3,\mathrm{final}}$ was taken as

$$c_{3,\mathrm{final}} = c_3(x,t) + c_3(2L-x,t) \quad (12)$$

The second term in the above equation simulates a mirror source at $x = 2L$, where L is the finite film thickness. Hence, at $x = L$, the flux is zero and the nonzero ^{2}H signal is obtained due to the reflection from the substrate. Note that the diffusion coefficient is the same for both the terms in eq 12. Figure 6 shows a typical diffusion profile along with the fits using eqs 34 and 35. The annealing of this sample was carried out at 150 °C for 7 h.

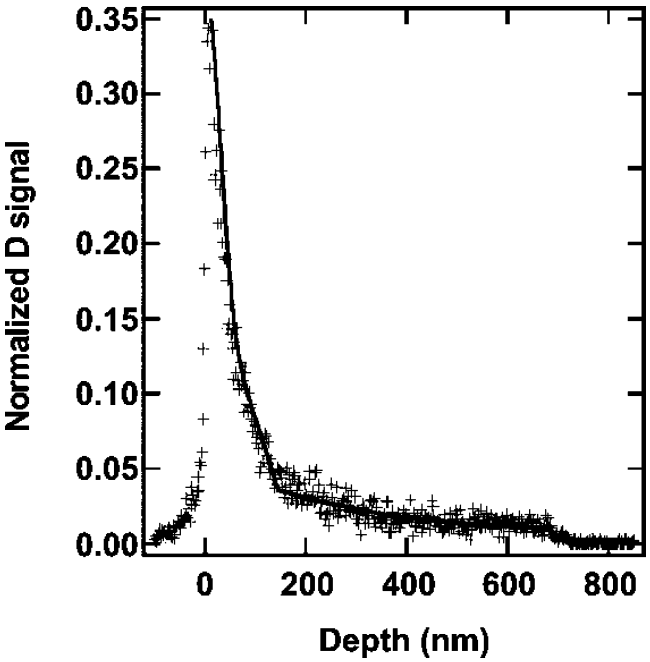

Figure 6. SIMS depth profile of SdESdES pentablock copolymer diffusing through an ordered cylindrical domain structure of SESES with a mixed orientation of the cylindrical axes (Figure 3). The block copolymer was allowed to diffuse at 150 °C for 7 h. The solid line from 10 to 140 nm is the best fit using eq 6, and from 140 nm onward, the fit is obtained using eq 7.

Figure 7 shows the diffusion coefficients as a function of temperature for the three cases: $D_{\mathrm{par,SESES}}$ (parallel diffusion), $D_{\mathrm{per,SESES}}$, and $D_{\mathrm{per,SES}}$ (perpendicular diffusion of the SESES and SES block copolymers, respectively). The plot shows that at the same temperature the higher molecular weight SESES pentablock copolymer diffuses faster than the SES triblock copolymer. This result is similar to the observation of Yokoyama and Kramer[18] for spherical domain triblock and diblock copolymers. In that case, triblock copolymers with sphere-forming end blocks diffused much faster than diblock copolymers of the same molecular weight. In order to understand this behavior, the perpendicular diffusion in a pentablock copolymer must be considered. As is the case for the triblock copolymer, a hopping diffusion mechanism with a thermodynamic barrier is expected for pentablock copolymer chains. However, the presence of two blocks of the minority block PE in the pentablock architecture gives rise to the possibility of two diffusion mechanisms. Yokoyama and Kramer[18] suggested these two mechanisms for a PVP−PS−PVP triblock copolymer with a spherical morphology where the PVP end blocks form the minority components. The case is analogous to the pentablock

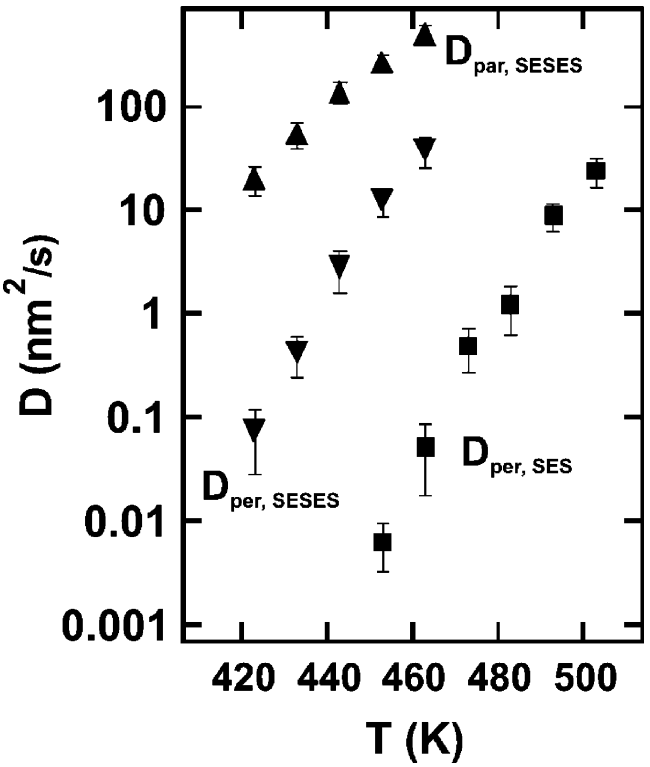

Figure 7. Self-diffusion coefficients as a function of temperature for parallel diffusion (▲) and perpendicular diffusion (▼) in SESES pentablock copolymer and perpendicular diffusion in SES triblock copolymer (■).

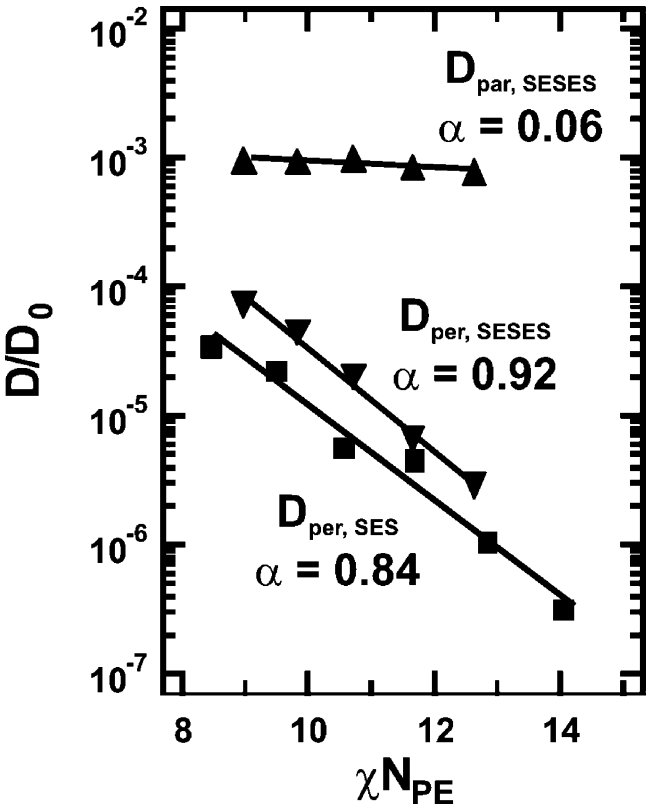

Figure 8. χN_{PE} dependence of the normalized self-diffusion coefficients D/D_0 for parallel diffusion of SESES (▲), walking diffusion of SESES (▼), and hopping diffusion of SES (■). The solid lines are fits using eq 3. The error bars are shown in Figure 7.

copolymer under investigation here since the minority component has two blocks per chain. The first one is the double-activation mechanism which involves the simultaneous activation of both the blocks from their respective cylinder cores into neighboring ones. The thermodynamic barrier for such a mechanism would be $2\chi N_{PE}$, where N_{PE} is the length of a single PE block. The factor of 2 is due to the presence of two such PE blocks. The other mechanism is "walking" diffusion where diffusion is accomplished by the activation of just one PE block at a time. The thermodynamic barrier for this mechanism is merely χN_{PE}. Figure 8 shows a plot of $\ln(D/D_0)$ as a function of χN_{PE} for the perpendicular diffusion in SES and SESES and parallel diffusion in SES. The best fit for D_{per} in the pentablock copolymer is obtained for $\alpha \sim 0.92$. The proximity of the value of α to one suggests that the "walking" diffusion mechanism is adopted by the pentablock copolymer chains. The activation barrier is a product of $\chi(T)$ and the length of the minority block. The presence of two blocks in the pentablock architecture, as opposed to a single block in the triblock architecture, reduces the barrier for the activated hopping of a single block, i.e., χN_{PE}, since in the pentablock copolymer architecture N_{PE} is reduced for similar (or less than double) total block copolymer M_ws when compared to the triblock copolymer architecture.

Hence, higher diffusion coefficients are observed for the pentablock copolymer at the same χ or T. Moreover, the difference in diffusion coefficients $D_{per,SESES}$ and $D_{per,SES}$ are small for the same value of χN_{PE} (Figure 8) which highlights the universal dependence of diffusion kinetics on the thermodynamic barrier χN_{PE} for the activated hopping mechanism. The reason for this difference between the perpendicular diffusion coefficients for the triblock and pentablock copolymers (at the same value of χN_{PE}) will be discussed in more detail at the end of this section.

It is clear from Figure 7 that the parallel diffusion is faster than the perpendicular diffusion at the same temperature in SESES pentablock copolymer. The fact that faster diffusion is observed at the same temperatures for the same block copolymer suggests that the activation barrier for parallel diffusion is lower than that for perpendicular diffusion. Moreover, a plot of D_{par}/D_0 as a function of χN_{PE}, as is shown in Figure 8, shows that the diffusion is practically independent of the thermodynamic barrier for hopping/walking diffusion ($\alpha \sim 0.03$). Parallel diffusion in unentangled systems is similar to the diffusion of a polymer chain in the absence of a thermodynamic barrier ($\chi \rightarrow 0$). The block copolymer chain diffuses along the interface without mixing the two blocks,[27,28] However, if that were the case in this system, the values of D_{par} would be similar to D_0. Evidently, this is not true since $D_{par}/D_0 \sim 10^{-3}$. This suggests that entanglements in the PE phase affect the parallel diffusion. For parallel diffusion in entangled systems, the mechanism of block retraction (as described in the Introduction) has been suggested for both lamellar[8] and cylindrical diblock copolymers.[14] The diffusion mechanism involves the retraction of the blocks to the interfacial region followed by the reinsertion into the respective domains. The barrier for diffusion depends on the length of the more entangled block and is given by the following equation:

$$D = D_0 \exp\left(-\xi\gamma \frac{N_B}{N_E}\right) \tag{13}$$

where N_B and N_E are the block lengths and the entanglement length of the more entangled block (PE in this case), respectively. γ is the fraction of this block that extends from the interfacial region into the pure block and ξ is a constant.

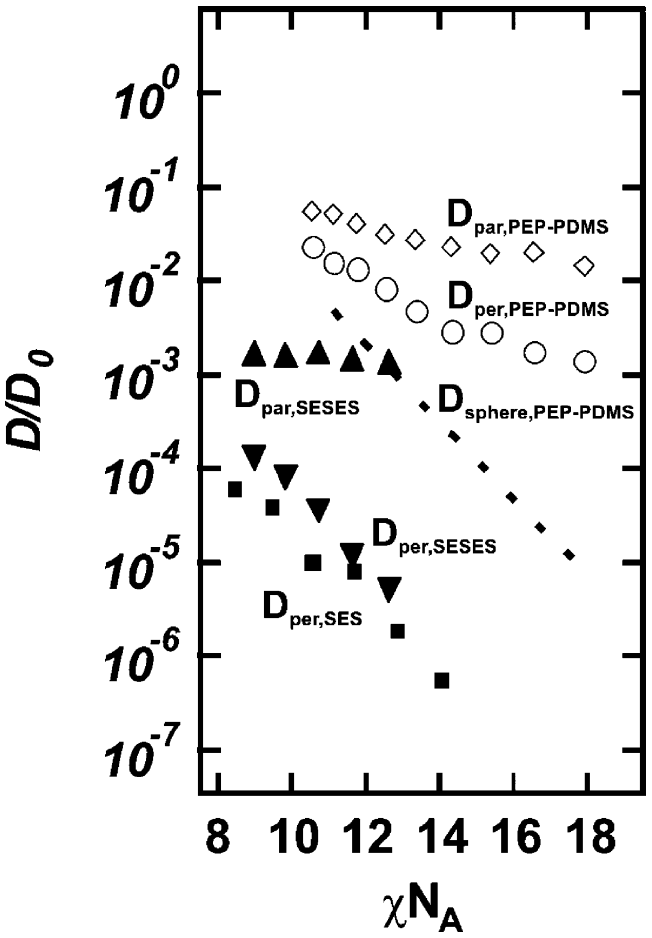

Figure 9. Universal χN_A dependence of the normalized self-diffusion coefficients D/D_0 for parallel diffusion of SESES (▲), walking diffusion of SESES (▼), and hopping diffusion of SES (■) plotted alongside the data from Lodge and Cavicchi for a PEP−PDMS diblock copolymer.[14] Parallel diffusion in PEP−PDMS diblock copolymer (◇), perpendicular diffusion in PEP−PDMS diblock copolymer with defects (○), and theoretical prediction for perpendicular diffusion in PEP−PDMS diblock copolymer with perfectly aligned cylinders (···). The last case (···) is equivalent to the diffusion in bcc spheres. N_A is the length of the minority block.

In the case of SESES pentablock copolymer, if block retraction does occur, the PE midblock loops must retract to the PE cylinder interface. However, such a PE loop cannot be significantly entangled with other loops if retraction is to be possible. Hence, only a small number of possible loop configurations are capable of retracting. Figure 9 shows a comparison of our data for SES triblock copolymer and SESES pentablock copolymer with the data obtained by Cavicchi and Lodge[14] for a cylinder-forming PEP−PDMS diblock copolymer ($M_n = 30$K g/mol, $f_{PEP} = 0.79$). The trends that we observe for parallel and perpendicular diffusion are qualitatively similar to theirs. However, for the SES and SESES block copolymers, the normalized diffusion coefficients are reduced by at least 2 orders of magnitude compared to the PEP−PDMS diblock copolymer. Since the offset between the two sets of data is independent of temperature and is observed for both parallel and perpendicular diffusion, it is suggestive of a mechanism inherent to the structure of the SES triblock copolymer and SESES pentablock copolymer. Moreover, this depression of the diffusion coefficients for our system is observed in spite of the fact that the entangled PEP block in their studies is more entangled ($N/N_e \sim 15$) than the entangled PE block in our studies ($N/N_e \sim 9$). As discussed before, for parallel diffusion the entangled PE midblock has to retract to the interface. In order to accomplish this, it has to form loops between two PS blocks. The loops have to be in a favorable conformation in order for this chain retraction to occur. Since many more PE midblock conformations are possible that do not allow such retraction, midblock retraction imposes an additional entropic penalty, over and above that from an end block. The same argument must also hold for perpendicular diffusion. No such constraint exists for the PEP−PDMS diblock copolymer architecture. The minority block, i.e., PDMS, is not pinned at its ends. Moreover, perpendicular diffusion in the PEP−PDMS system occurs via retraction of the unentangled PDMS chains, which form the cylinder cores. The absence of the looping constraint along with the relative ease with which the unentangled PDMS block can hop from one cylinder to another may explain the higher values of the diffusion coefficients in that system compared to the SES and SESES systems. Last, the lower values of $D_{per,SES}$ relative to $D_{per,SESES}$ may also be explained if the length of the PE blocks in the triblock and pentablock copolymers is considered. In the SES triblock copolymer, the PE block has a length of about 12 500 g/mol, which makes it more entangled ($N/N_e \sim 12.5$) as compared to the PE block in the SESES pentablock copolymer ($N/N_e \sim 9$). The increased number of entanglements impose a higher entropic constraint on the PE block in the SES triblock copolymer as compared to the PE block in the SESES pentablock copolymer. This extra constraint due to the longer PE block may be the reason why slower diffusion is observed in the perpendicular direction for the SES triblock copolymer as compared to the SESES pentablock copolymer (even though they show about the same slope in the plot of $\log(D/D_0)$ vs χN_{PE}, as shown in Figures 8 and 9).

Conclusion

The present work demonstrates the effect of chain architecture on the diffusion kinetics of poly(styrene)−poly(ethylene) triblock and pentablock copolymers. A hopping diffusion mechanism is observed for the triblock copolymer where the single PE block hops from one cylindrical domain to another after overcoming the thermodynamic barrier χN_{PE}. The pentablock copolymer diffuses by the walking mechanism which involves the thermodynamic activation of a single block of poly(ethylene) and not the simultaneous activation of both PE blocks (in SESES). This suggests that when the pentablock has a comparable or higher (but less than double) molecular weight than the triblock copolymer, it will exhibit faster diffusion kinetics due to a lower barrier. Last, the change in microdomain orientation with depth (from parallel cylinders to perpendicular) allows us to make a comparison between parallel and perpendicular diffusion for the pentablock copolymer. It is observed that parallel diffusion in pentablock copolymers is faster than perpendicular diffusion and relatively independent of the activation barrier χN_{PE}. However, the values of the parallel diffusion coefficients are about 3 orders of magnitude lower than those of PS homopolymer. We believe that the looping of the highly entangled PE block (due to the triblock and pentablock architecture) puts entropic constraints on the pullout of this block. These entropic constraints are independent of temperature and diffusion direction and hence cause a uniform reduction in both parallel and perpendicular diffusion coefficients relative to diffusion coefficients in systems where the minority blocks are not constrained.

Acknowledgment. The authors thank Prof. Glenn Fredrickson and Gila Stein for useful discussions. The work was supported by the NSF-Polymers Program Award DMR0307233 and by a gift from Dow Chemical Co. This work made use of

MRL Central Facilities supported by the MRSEC Program of the National Science Foundation under Award DMR05-20415. The use of APS at ANL is supported by the U.S. Department of Energy under Contract DE-AC02-06CH11357.

Appendix

The system of differential equations for the schematic shown in Figure 5 is as follows:

$$\frac{\partial c_1}{\partial t} = D_1 \frac{\partial^2 c_1}{\partial x^2} \qquad 0 \le x \le h \tag{14}$$

$$\frac{\partial c_2}{\partial t} = D_1 \frac{\partial^2 c_2}{\partial x^2} \qquad h \le x \le l \tag{15}$$

$$\frac{\partial c_3}{\partial t} = D_3 \frac{\partial^2 c_3}{\partial x^2} \qquad l \le x < \infty \tag{16}$$

where D_1 and D_3 are the diffusion coefficients from 0 to l and from l to ∞, respectively. The following boundary conditions can be applied to solve the above system of equations:

$$c_1 = c_0 \qquad t = 0,\ 0 \le x \le h \tag{17}$$

$$\frac{\partial c_1}{\partial x} = 0 \qquad x = 0,\ t > 0 \tag{18}$$

$$c_1 = c_2 \qquad x = h,\ t > 0 \tag{19}$$

$$\frac{\partial c_1}{\partial x} = \frac{\partial c_2}{\partial x} \qquad x = h,\ t > 0 \tag{20}$$

$$c_2 = c_3 \qquad x = l,\ t > 0 \tag{21}$$

$$D_1 \frac{\partial c_2}{\partial x} = D_3 \frac{\partial c_3}{\partial x} \qquad x = l,\ t > 0 \tag{22}$$

$$c_3 = 0 \qquad x \to \infty \tag{23}$$

The Laplace transformation is used to transform eqs 14−16 to a system of ordinary differential equations. The Laplace transformation transforms $c(x,t)$ to $\bar{c}(x)$. The transformation is written as follows:

$$L\{c(x,t)\} = \bar{c} = \int_0^\infty e^{-pt} c(x,t)\, dt \tag{24}$$

where p is a number whose real part is positive and large enough to make the integral convergent. Using eq 17, the Laplace transformation of eq 14 becomes

$$\frac{\partial^2 \bar{c}_1}{\partial x^2} - {q_1}^2 \bar{c}_1 = -\frac{c_0}{D_1} \qquad 0 \le x \le h \tag{25}$$

Equations 15 and 16 are transformed to the form

$$\frac{\partial^2 \bar{c}_2}{\partial x^2} - {q_1}^2 \bar{c}_2 = 0 \qquad h \le x \le l \tag{26}$$

$$\frac{\partial^2 \bar{c}_3}{\partial x^2} - {q_3}^2 \bar{c}_3 = 0 \qquad l \le x < \infty \tag{27}$$

q_1 and q_3 are defined as

$$q_1 = \sqrt{\frac{p}{D_1}} \tag{28}$$

$$q_3 = \sqrt{\frac{p}{D_3}} \tag{29}$$

Equations 25−27 are a system of ordinary differential equations with the general solutions:

$$\bar{c}_1 = A_1 e^{q_1 x} + B_1 e^{-q_1 x} + \frac{c_0}{p} \tag{30}$$

$$\bar{c}_2 = A_2 e^{q_1 x} + B_2 e^{-q_1 x} \tag{31}$$

$$\bar{c}_3 = A_3 e^{q_3 x} + B_3 e^{-q_3 x} \tag{32}$$

Equations 18 and 23 reduce the above system of equations to the following form:

$$\bar{c}_1 = A_1 (e^{q_1 x} + e^{-q_1 x}) + \frac{c_0}{p} \tag{33}$$

$$\bar{c}_2 = A_2 e^{q_1 x} + B_2 e^{-q_1 x} \tag{34}$$

$$\bar{c}_3 = B_3 e^{-q_3 x} \tag{35}$$

The above set of equations consists of four variables, A_1, A_2, B_2, and B_3. Using the remaining four boundary conditions 19−22, they can be solved for as four simultaneous equations to get:

$$A_1 = \frac{-c_0}{2p}\left[\frac{e^{-q_1(h-l)} + \alpha_{an} e^{q_1(h-l)}}{e^{q_1 l} + \alpha_{an} e^{-q_1 l}}\right] \tag{36}$$

$$A_2 = \frac{c_0 \alpha_{an} e^{-2q_1 l}}{2p}\left[\frac{e^{-q_1 h} - e^{q_1 h}}{1 + \alpha_{an} e^{-2q_1 l}}\right] \tag{37}$$

$$B_2 = \frac{c_0}{2p}\left[\frac{e^{q_1 h} - e^{-q_1 h}}{1 + \alpha_{an} e^{-2q_1 l}}\right] \tag{38}$$

$$B_3 = \frac{k c_0 \alpha_{an} e^{-2q_1 l}}{p(1-k)}\left[\frac{e^{-q_1 h} - e^{q_1 h}}{1 + \alpha_{an} e^{-2q_1 l}}\right] e^{(q_1+q_3)l} \tag{39}$$

where α_{an} and k are defined as

$$\alpha_{an} = \frac{1-k}{1+k} \tag{40}$$

$$k = \sqrt{\frac{D_1}{D_3}} \tag{41}$$

Substituting for A_2, B_2, and B_3 in eqs 34 and 35 and simplifying

$$\bar{c}_2 = \frac{c_0}{2p}\left[\frac{e^{-q_1(x-h)} - e^{-q_1(x+h)} + \alpha_{an}(e^{-q_1(2l+h-x)} - e^{-q_1(2l-h-x)})}{1 + \alpha_{an} e^{-2q_1 l}}\right] \tag{42}$$

$$\bar{c}_3 = \frac{-c_0 k}{p(1+k)}\left[\frac{e^{-q_1(L+h)-q_3(x-l)} - e^{-q_1(l-h)-q_3(x-l)}}{1 + \alpha_{an} e^{-2q_1 l}}\right] \tag{43}$$

Using the binomial theorem, the denominator can be expanded into a series and introduced into the numerator:

$$\frac{1}{1+\alpha_{an}e^{-2q_1l}} = \sum_{n=0}^{\infty}(-\alpha_{an})^n e^{-2nq_1l} \tag{44}$$

Therefore, eqs 42 and 43 become

$$\bar{c}_2 = \frac{c_0}{2p}\sum_{n=0}^{\infty}(-\alpha_{an})^n(e^{-q_1(2nl+x-h)} - e^{-q_1(2nl+x+h)} + \alpha_{an}e^{-q_1(2(n+1)l-x+h)} - \alpha_{an}e^{-q_1(2(n+1)l-x-h)}) \tag{45}$$

$$\bar{c}_3 = \frac{-c_0k}{p(1+k)}\sum_{n=0}^{\infty}(-\alpha_{an})^n(e^{-q_1((2n+1)l+h)-q_3(x-l)} - e^{-q_1((2n+1)l-h)-q_3(x-l)}) \tag{46}$$

The above solutions are the Laplace transformations of c_2 and c_3 with p ($= q_i^2D_i$) as the operator. A standard inverse Laplace transformation can be performed to functions of the form above:

$$\text{inverse}\left(\frac{1}{p}e^{-K\sqrt{p}}\right) = \text{erfc}\left(\frac{K}{2\sqrt{t}}\right) \tag{47}$$

By performing this inversion on eqs 45 and 46, the solutions c_2 and c_3 are obtained:

$$c_2(x,t) = -\frac{c_0}{2}\left[\text{erf}\left(\frac{h+x}{2\sqrt{D_1t}}\right) + \text{erf}\left(\frac{h-x}{2\sqrt{D_1t}}\right) - \sum_{n=0}^{\infty}(-\alpha_{an})^n\left\{\text{erf}\left(\frac{2nl+h+x}{2\sqrt{D_1t}}\right) + \text{erf}\left(\frac{2nl+h-x}{2\sqrt{D_1t}}\right) - \text{erf}\left(\frac{2nl-h+x}{2\sqrt{D_1t}}\right) - \text{erf}\left(\frac{2nl-h-x}{2\sqrt{D_1t}}\right)\right\}\right] \tag{48}$$

$$c_3(x,t) = \frac{c_0k}{1+k}\sum_{n=0}^{\infty}(-\alpha_{an})^n\left\{\text{erf}\left(\frac{(2n+1)l+h}{2\sqrt{D_1t}} + \frac{x-l}{2\sqrt{D_3t}}\right) - \text{erf}\left(\frac{(2n+1)l-h}{2\sqrt{D_1t}} + \frac{x-l}{2\sqrt{D_3t}}\right)\right\} \tag{49}$$

As a check for the solution, by substituting $\alpha_{an} = 0$ (i.e., the case for no diffusion anisotropy) in eqs 48 and 49, the general solution to the diffusion equation is obtained, i.e.

$$c = \frac{c_0}{2}\left[\text{erf}\left(\frac{h+x}{2\sqrt{Dt}}\right) + \text{erf}\left(\frac{h-x}{2\sqrt{Dt}}\right)\right] \tag{50}$$

where $D = D_1 = D_3$.

References and Notes

(1) Bates, F. S.; Fredrickson, G. H. *Phys. Today* **1999**, *52*, 32.
(2) Matsen, M. W.; Bates, F. S. *Macromolecules* **1996**, *29*, 1091.
(3) Bates, F. S.; Fredrickson, G. H. *Annu. Rev. Phys. Chem.* **1990**, *41*, 525.
(4) Milner, S. T.; Fredrickson, G. H. *MRS Symp. Proc., Macromol. Liq.* **1990**, *177*, 169.
(5) Barrat, J. L. Fredrickson, G. H. *Macromolecules* **1991**, *24*, 6378.
(6) Shull, K. R.; Kramer, E. J.; Bates, F. S.; Rosedale, J. H. *Macromolecules* **1991**, *24*, 1383.
(7) Dalvi, M. C.; Lodge, T. P. *Macromolecules* **1993**, *26*, 859.
(8) Lodge, T. P.; Dalvi, M. C. *Phys. Rev. Lett.* **1995**, *75*, 657.
(9) Helfand, E. *Macromolecules* **1992**, *25*, 492.
(10) Murat, M.; Grest, G. C.; Kremer, K. *Europhys. Lett.* **1998**, *42*, 401.
(11) Lodge, T. P.; Hamersky, M. W.; Milhaupt, J. M.;Kannan, R. M.; Dalvi, M. C.; Eastman, C. E. *Macromol. Symp.* **1997**, *121*, 219.
(12) Hammersky, M. W.; Hillmyer, M. A.; Tirrell, M.; Bates,F. S.; Lodge, T. P.; von Meerwall, E. D. *Macromolecules* **1998**, *31*, 5363.
(13) Vogt, S.; Jian, T.; Anastasiadis, S. H.; Fytas, G.; Fischer, E. W. *Macromolecules* **1993**, *26*, 3357.
(14) Cavicchi, K. A.; Lodge, T. P. *Macromolecules* **2004**, *37*, 6004.
(15) Yokoyama, H.; Kramer, E. J. *Macromolecules* **1998**, *31*, 7871.
(16) Yokoyama, H.; Kramer, E. J.; Rafailovich, M. H.;Sokolov, J.; Schwarz, S. A. *Macromolecules* **1998**, *31*, 8826.
(17) Yokoyama, H.; Kramer, E. J.; Hajduk, D. A.; Bates, F. S. *Macromolecules* **1999**, *32*, 3353.
(18) Yokoyama, H.; Kramer, E. J. *Macromolecules* **2000**, *33*, 954.
(19) Yokoyama, H.; Kramer, E. J.; Fredrickson, G. H. *Macromolecules* **2000**, *33*, 2249.
(20) Yokoyama, H.; Kramer, E. J. *Macromolecules* **2000**, *33*, 1871.
(21) Khanna, V.; Ruokolainen, J.; Kramer, E. J.; Hahn, S. F. *Macromolecules* **2006**, *39*, 4480.
(22) Han, C. D.; Choi, S.; Lee, K. M.; Hahn, S. F. *Macromolecules* **2004**, *37*, 7290.
(23) Pearson, D. S.; Ver Strate, G.; von Meerwall, E.; Schillingld, F. C. *Macromolecules* **1987**, *20*, 1133.
(24) Green, P. F.; Kramer, E. J. *J. Mater. Res.* **1986**, *1*, 202.
(25) Khanna, V.; Cochran, E. W.; Hexemer, A.; Stein, G. E.; Fredrickson, G. H.; Kramer, E. J.; Li, X.; Wang, J.; Hahn, S. F. *Macromolecules* **2006**, *39*, 9346.
(26) Dee, G. T.; Sauer, B. B. *J. Colloid Interface Sci.* **1992**, *152*, 85.
(27) Eastman, C. E.; Lodge, T. P. *Macromolecules* **1994**, *27*, 5591.
(28) Hamersky, M. W.; Tirrell, M.; Lodge, T. P. *Langmuir* **1998**, *14*, 6974.

MA061703P